

IN-SITU QUALITY INSPECTION OF LASER POWDER-BED FUSION USING HIGH-RESOLUTION VISUAL CAMERA IMAGES

Masoumeh Aminzadeh, Thomas Kurfess

Woodruff School of Mechanical Engineering, Georgia Institute of Technology, Atlanta, GA
30332

Abstract

Issues of part quality in terms of quality of fusion and formed porosity are widely known and stated as some of the important challenges with laser powder-bed fusion (LPBF) process. This paper addresses the in-situ inspection of layer-wise part quality using visual camera images. High-resolution visual images are captured from each layer of the part during LPBF process. The imaging and illumination setups are developed such that the produced images visualize detailed surface characteristics of each layer of the build such as fused seams, as well as the individual formed pores. To enable automated inspection of these images, appropriate image processing algorithms are developed to detect individual pores formed in each layer. In addition to detection of individual pores, intelligent pattern matching algorithms are developed, trained, and implemented to identify porous regions from non-porous layers. The surface characteristics of the layers as visualized in camera images can also provide a measure of quality of fusion and the energy of the layer, and an estimated level of porosity. Discussion on characterization of the surface quality in terms of roughness, quality of fusion, and the energy of the build will be made. The results of the automated image analyses provide useful feedback for in-situ process modification as well as part quality assessment.

Introduction

The need for developing techniques and approaches to improve and control the quality of parts made by metal powder-bed additive manufacturing (AM) is widely known and stated. The high chances of formation of pores in metal AM techniques such as laser powder-bed fusion (LPBF) can lead to fabrication of parts that do not meet the requirements for quality and structural properties. Therefore, to assure the quality of parts, it is required to develop strategies to monitor and control formation of defects and pores in the part, especially in an in-situ fashion during the build.

The majority of the past work on quality control in metal AM focuses on real-time process control as a means to control the physical phenomena associated with powder fusion process and consequently prevent formation of pores. However, despite partial improvements achieved by real-time process control, due to the high level of complexity of powder fusion process and its governing factors, defects and pores still form in the parts. Therefore, an alternative or complementary approach is sought which is based on directly monitoring or inspection of the defects such as pores. The results of defect inspection can then help with making decisions regarding the acceptance of the built portion of the part, process control, and taking corrective actions to fix the defects if possible.

While measurements such as 2D thermal data or acoustic waves might provide insight into the quality of the part, 2D visual camera images have the capability to visualize defects as well as individual pores provided appropriate illumination arrangements and setup. There is a very limited number of work on in-situ inspection in metal AM, or specifically powder-bed AM, using visual camera images. Craeghs *et al.*, [1], used a visual camera to build a powder deposition monitoring system in L-PBF. They detected the effect of a worn or damaged coater that can be regarded as specific type of process error that can lead to part defects. Kleszczynski *et al.*, [2], used a 29 megapixel visual camera mounted outside the machine to visually examine process errors in EBM. They studied the effect of factors such as input energy on formation of elevations at edges which they manually observed in high-resolution camera images. In another subsequent work, [3, 4], they used their imaging system to capture images with 24 $\mu\text{m}/\text{pixel}$ on-part resolution to inspect elevations in the part. They captured camera images from the deposited powder layer and used constant value thresholding to detect elevated regions in the part.

Aminzadeh *et al.*, [5, 6], proposed a framework based on machine vision for inspection of geometric errors as well as pores; they designed and implemented image processing algorithms to automatically detect the geometric errors and inspect the dimensional accuracy of the part from high-resolution camera images. In a subsequent work, [7], they used a 9 megapixel visual camera mounted inside the build chamber perpendicular to the build platform that provided images with sufficient contrast between the powder and fused regions at a very detailed 7 $\mu\text{m}/\text{pixel}$ on-part resolution. They developed automatic image segmentation algorithms that detected the geometric cross section of the parts with 80 μm detection error which was smaller than the laser scan diameter.

Foster *et al.* [8], used a 29 megapixel camera mounted inside the machine at an angle from the build platform. They were able to capture images with 50 $\mu\text{m}/\text{pixel}$ resolution and 15 $\mu\text{m}/\text{pixel}$ resolution depending on the utilized camera lens. The fused regions are visualized with relatively low contrast in the captured images. However, despite the high resolution, the formed defects and detailed surface characteristics were not yet visible in the images. They studied the effect of illumination on image characteristics to provide images that can later be used for in-situ inspection purposes.

This paper describes the system and the work on development of a new imaging setup with the collaboration of the Edison Welding Institute (EWI) at EWI. Unlike the previous and existing work on development of imaging setup for powder-bed AM, this system resolves, to a significant extent, the challenges associated with the illumination and captures images that visualize detailed surface features such as individual pores as they appear in microscopic images. Appropriate image processing algorithms are then developed to detect pores from the part surface automatically. In addition to detection of individual pores, an intelligent classification algorithm is developed to identify porous versus non-porous layers.

Imaging Setup and Discussion on Images Characteristics

Figure 1 shows a close-up of the build chamber of a selective laser melting (SLM) machine that was built and customized at EWI. An IPG 600 watt single mode fiber laser was used as the laser source. As seen in the Figure, in this customized machine, the laser source is mounted with some shift to the left at the top of the build platform. This feature provides room right at the top of the build platform for mounting sensors.

An 8.8 megapixel USB Digital Camera with high focus lenses was mounted directly at the top of the build platform looking down perpendicular to the build. The camera resolution and the captured image size is 4096×2160 pixels. The following features of this imaging setup are noteworthy. The camera is mounted inside the machine right at the top of the build platform. This significantly reduces the distance between the camera and the build platform. Utilizing lenses with a small focal length would allow capturing images with very high on-part resolution in order of several micron pixel size. Additionally, the camera captures pictures at a perpendicular angle from the build platform which results in no perspective effects. Consequently, the picture is uniformly scaled throughout the image with the same pixel size all over the image. Therefore, there would be no need for camera calibration to fix for shape and size distortions due to perspective effects. Camera calibration would have added more computational complexity and would introduce new errors and uncertainties due to machine vibration [9].

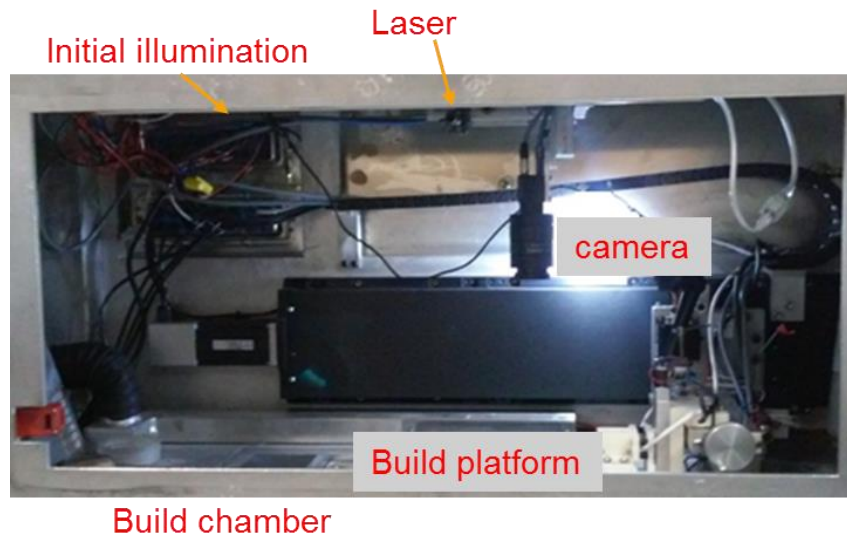


Figure 1- Close up of the build chamber of the machine and its components.

The other important component of the imaging setup in addition to the camera is the illumination (light) source. The location and orientation of the camera and the light source play critical role in the quality of imaging. The best orientation for the camera is perpendicular to the build to remove the perspective effects and the need for camera calibration that was met in this imaging setup. The camera was mounted conveniently on a stationary fixture connected to the wall of the chamber. It was mounted such that it doesn't block the laser path. It was later examined that the distance of the camera from the build in this setup is not optimal and better image might be captured if the camera be put somewhat closer to the build depending on the lens focal length.

However, this current position for camera was mainly determined based on the physical limitations.

To mount the light source, initially a single light source in form of an adjustable, white, high intensity LED spot light, was mounted at the top of the build platform emanating at an angle, as shown in Figure 1. The level of brightness was adjusted until rather clear images of the powder bed could be captured. To examine image quality, builds with square cross sections were fabricated for several layers. Images were captured and acquired at each layer. Figure 2 shows an example of images captured with this illumination setup.

With an 8.8 megapixel camera with 4096×2160 pixel image sizes, the on-part pixel size for images was measured as 7 μm . Before using the 8.8 megapixel camera in this imaging setup at EWI, a 2 megapixel camera with 1080×1920 pixel image sizes was utilized that led to the on-part pixel size as 20 μm with the same camera mounting location. This is whereas the resolution achieved by Kleszczynski *et al.* [3, 9] with a 29 megapixel camera with image size of 4234×4234 pixels was 24 $\mu\text{m}/\text{pixel}$, and the resolution achieved by Foster *et al.* [8], using a 29 megapixel camera, reached 50 or 15 $\mu\text{m}/\text{pixel}$, depending on the utilized lens. This better resolution achieved in the imaging setup described in this work, 7 $\mu\text{m}/\text{pixel}$ using an 8.8 Megapixel camera, is due to the smaller distance of the camera from the build and the perpendicular view of the camera. It should also be mentioned that increasing the on-part resolution is achieved at the cost of reduction in the field of view of the camera. Given a 7 $\mu\text{m}/\text{pixel}$ resolution, the field of view of the camera was about 30 mm × 150 mm whereas the field of view in the imaging setup by Kleszczynski *et al.*, [2], is about 100 mm × 100 mm.

Defects such as pores formed in metal powder-bed AM can be as small as 20 μm in size, and pores as small as 100 μm are known to have effect on the part quality and structural properties. With a pixel size of 20 μm , pores of size 100 μm , may appear in only 5 pixels along the diameter. Objects of size 5 pixels may easily be produced due to noise, shades, or other non-defective surface features or discolorations. Therefore, for visualization of pores, a smaller pixel size, such as 7 μm , is required which captures a pore of 100 μm in about 15 pixels along the diameter. A 15 pixel object size provides enough visual features for human eyes to identify and distinguish from most other objects. A commercial standard microscope with image pixel size of 7 μm can clearly shows pores of and larger than 100 μm .

As seen in Figure 2, the image captured from the layer shows the fusion seams, fused surface and powder bed texture as well as the clear boundary of the fused object. The images provided rather sufficient clarity for segmentation and inspection of the fused region geometry [7]. However, throughout the fused region, there are several dark regions where the fused surface details are not visible. In fact, they may easily be confused with lack of fusion or defects. A subsequent microscopic examination from the layer, however, showed that these dark areas do not correspond to any defect or pore and are only formed due to shades and insufficient light reflected from those areas.

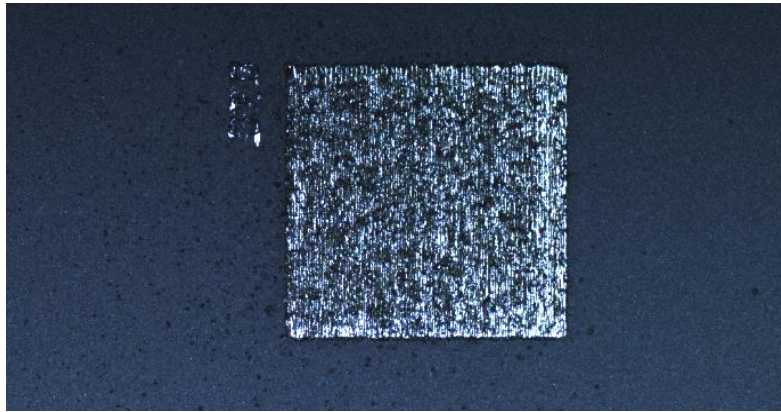


Figure 2- Example of image with the setup using 8.8 megapixel camera and adjusted level of intensity for LED spotlight mounted at an angle from the build.

To investigate visibility of pores in images, it is required to build layers that contain pores. Therefore, a range of process parameters including non-optimal parameters that are known to produce pores in parts were chosen. Microscopic examination was used to examine and confirm existence of pores in the parts. The target for the visual imaging system in this machine is then to visualize pores as they appear in high-resolution microscopic images. The resolution of the standard microscope is measured as $7\ \mu\text{m}/\text{pixel}$ which turns out to be equal to the camera on-part resolution but with a smaller field of view.

From comparison of the camera images by the setup with spot LED as in Figure 1 with microscopic images of the porous layers, it was seen that pores are not visualized in camera image whereas they are clearly visible in microscopic images (see Figure 3 (a) and (b) for example).

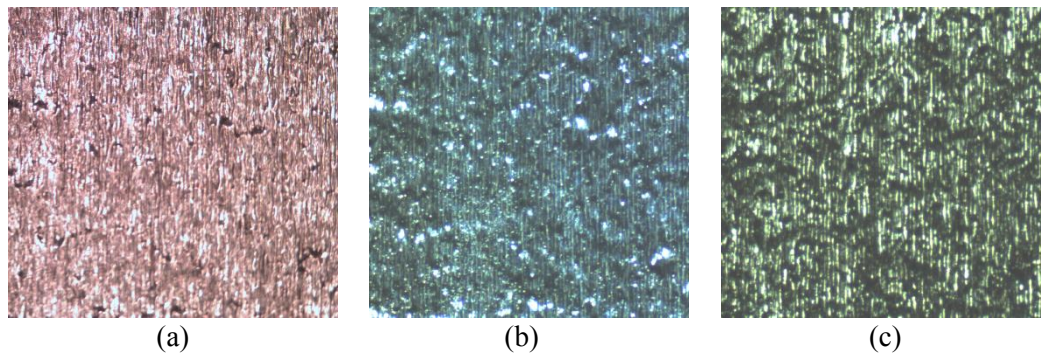


Figure 3- Images of the same build layer: (a) captured by a standard microscope with the resolution of $7\ \mu\text{m}/\text{pixel}$, (b) captured by visual camera in the imaging setup using the LED spot light at an angle (Figure 1) with the resolution of $7\ \mu\text{m}/\text{pixel}$, (c) captured by visual camera in the imaging setup using the ring LED perpendicular to the build and around the camera with the resolution of $7\ \mu\text{m}/\text{pixel}$.

The reason for invisibility of pores from camera images could be that insufficient illumination is reflected from pores into the camera. This could be due to large diffusivity and the non-uniform illumination from an angle, as well as the shades of surface elevations that cover the

pores. More uniform illumination should then be considered that can be provided by implementing two or more light sources from different sides to remove that shadows caused by each individual light source. An alternative more effective illumination would be to use a symmetric illumination such as a ring illumination mounted directly at the top of the build with light arrays perpendicular to the build platform. To provide a uniform, symmetric, and shadow-free illumination such as in microscopes, an adjustable microscope ring light for stereo microscope was used. The ring LED has 2-1/2" (64mm) inside diameter and 4" (100mm) outside diameter. The only place that the ring LED could be mounted, to avoid blockage of the laser beam, was around the camera at the same distance of the camera from the build. The operating distance of similar microscope lights are in the range of several inches, therefore, mounting the LED at this distance of about 1 ft from the part, resulted in dark and rather low-quality images and the problem with capturing dark non-illuminated areas within fused region persisted (see Figure 3 (c)). This problem was most visibly seen within the fused region that has a relatively rough surface and variations of height that can create shadows and prevent the light to be reflected from the surface uniformly. It was investigated and seen that this problem can be removed if the ring illumination is mounted closer to the build at a distance within 5 cm to 10 cm from the build. By having light reflected from the build surface uniformly and efficiently, the details of the build surface including surface roughness and height variation as well as pores could be visualized.

To mount the ring illumination closer to the build without blocking the laser beam, a ring illumination with a very large inside diameter would have been needed; however, a smaller ring illumination centered closely right on the examined area would be ideal for capturing clear well-lit images. Therefore, it was decided that illumination source would be mounted at a moving fixture so that it stays away as the laser is scanning and moves to the top of the build once the layer is built and is ready to take picture. Given the current mechanism, it was planned that the ring illumination source be mounted at a fixture connected to the coater and moves away as the coater passes. A fixture with three fixable multi-DoF joints was mounted on the coater (as in Figure 4). The ring LED was mounted on the coater and the fixture was adjusted such that the light would be at the desired distance with the build platform emanating light perpendicular to the platform. The machine was programmed such that after each layer is scanned or deposited using the laser, the coater would get back and stop at the position where the light is at the specified position and the camera would automatically picture from the layer at that stop.

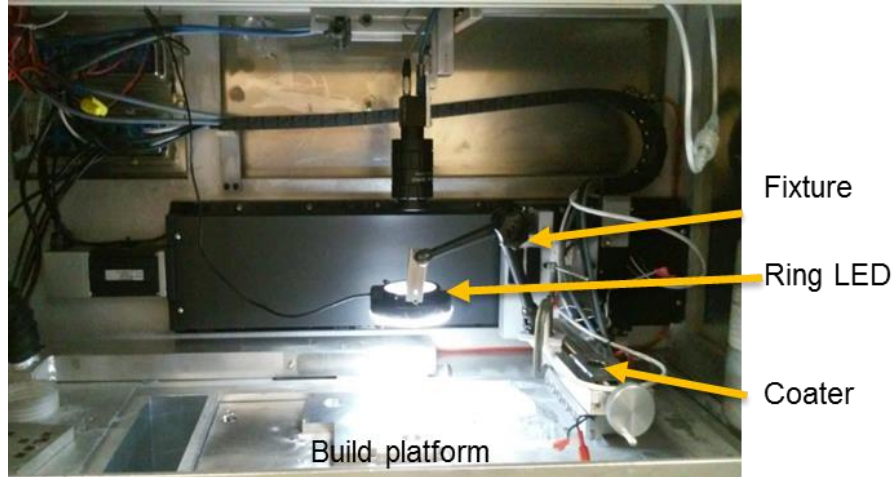


Figure 4- Image of the new imaging setup with movable ring LED mounted at a fixture on the coater at a selected height above the build platform.

To find an optimal distance for light source from the build platform and adjust the LED at that height, a series of trials and errors by varying the LED distance from the build as well as camera and light settings and parameters were conducted and images of parts were captured. Camera images were captured in-situ from each layer of several parts built at non-optimal parameters known to form pores. Microscopic images were then captured from the parts' surface (top layer) outside the machine. It was investigated for the light source mounted at a distance around 60-80 mm from the platform, the camera images captured from the parts show strong correspondence with microscopic images and visualize pores as they appear in microscopic images. This distance was marked and arrangements were planned to mount the light source at that distance from the build.

Figure 5 (a) shows an example image captured in situ by the new setup. Figure 5 (b) shows the corresponding microscopic image from the part. It can clearly be seen that the two images match well. Additionally the pores are visible in camera images as they appear in microscopic images.

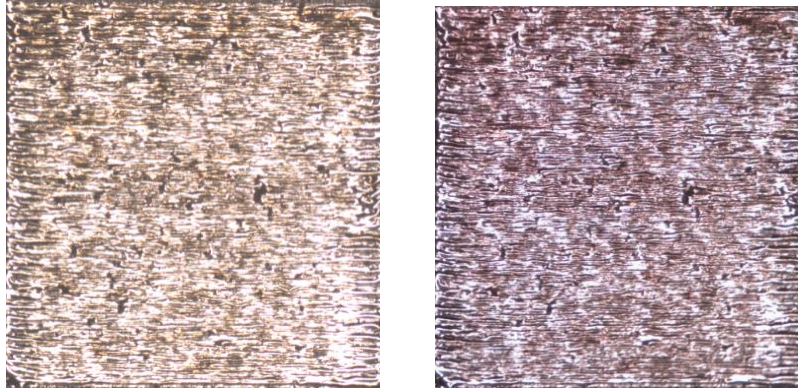


Figure 5- (a) An example image captured from a porous surface by the setup with movable ring LED (Figure 4), (b) corresponding microscopic image of the part.

It was also examined that mounting the camera closer to the build platform would also improve image quality. However, due to the physical limitations and to prevent camera vibration, and since the light source distance from the build had much more dominant effect, it was decided that camera would be remained mounted stably and fixed to the chamber wall.

In addition to the distance of the light source from the build, the ring LED is equipped with four zones to independently control light intensity and direction. The light condition with all four zones lit-up was also compared against only two opposite zones lit-up which the latter resembles the situation with two light source lighting up the part from opposite directions. It was seen the optimal light condition is when all four zones emanate the part uniformly from all directions.

In general, this imaging setup is a combination of selected camera settings, use of physical polarizer or filters, illumination intensity and settings, and the distance of the illumination source with the build surface. The most influential parameters are the distance of the illumination source and the camera exposure time; camera gain value and application of filters and polarizer have less important effect. These parameters were adjusted in an iterative manner such that the captured camera images look, to human eye, as much similar to microscopic images as possible. Note that in Figure 5 (a) the color temperature of the camera has been increased (i.e. images are red rather than blue as in Figure 2 and Figure 3 (b) and (c)).

Although the camera images visualized pores and showed overall good agreements with microscopic images, the camera images still do not show a clear and high-quality picture of the part surface as microscopic images. Further pictures of the surface of the parts were taken after the build and were examined in comparison with their corresponding microscopic images, the reasons for some of the mismatch were later identified and here the main ones can be described as follows: 1) The microscope can be focused very sharply at the top layer within several microns such that extrusions of one layer below are too blurry and are barely seen in the microscopic image. However, after the camera was focused, it was seen the camera is not focused precisely at the top layer within several microns; in other word, in camera images captured after removal of the powder, extrusions from a layer below were seen as sharp as the features on the top layer (see Figure 6). 2) The high reflectivity of the metallic surface in some regions led to saturations that covered the underneath as well as nearby surface (see Figure 7).

Lack of a sharp focus on an image in fact acts like a low-pass filter that removes or blurs the sharp and small features associated with low-frequency. Therefore, the color value captured by a pixel is, in fact, affected by the color value (light) from both the location corresponding to that pixel and its neighboring regions. This may cause the images to show some spots darker than they truly are, looking like pores, or slightly distort shapes of some pores. It may additionally lead to larger saturation regions in the image as pixels receive light from the neighborhood of their corresponding spacial point and pixels that otherwise would not have been saturated, saturate and are considered as missing data (see Figure 7).

The two aforementioned problems could be alleviated by further and more detailed modification of camera and ring LED. Overall, current camera images can show individual pores that agree with microscope and the agreement almost holds for any pore larger than 100 microns.

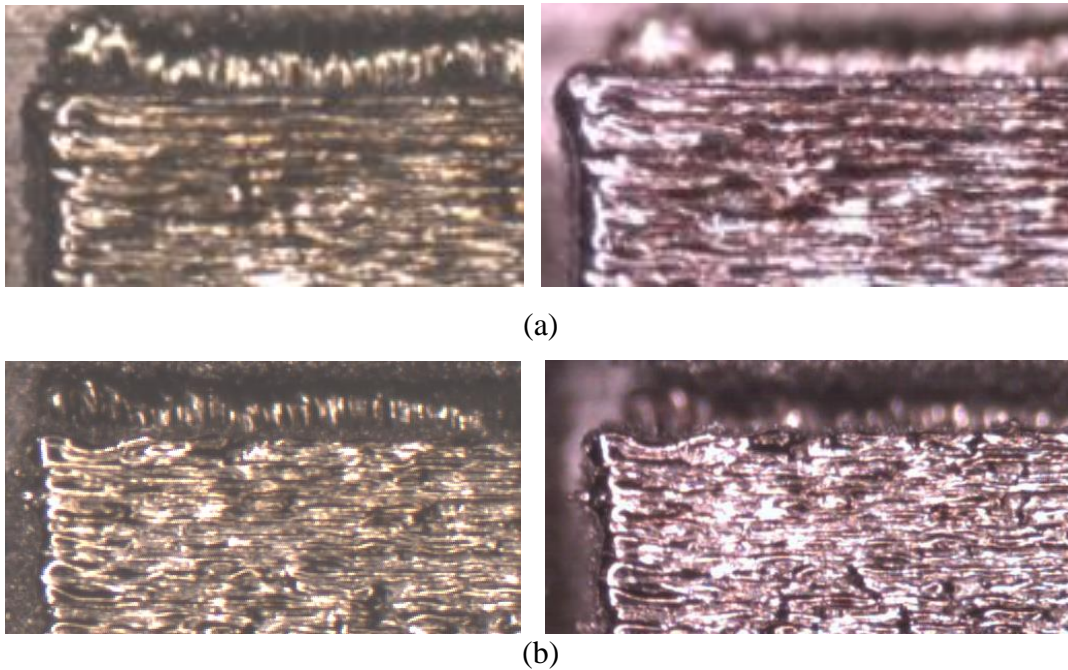


Figure 6- Illustration of the sharp focus of camera with respect to microscope. Comparison of the zoomed-in views of image from camera from a part after build (left in each row) and corresponding microscope image (right in each row). Each row shows the same part within the row that is different from the other row.

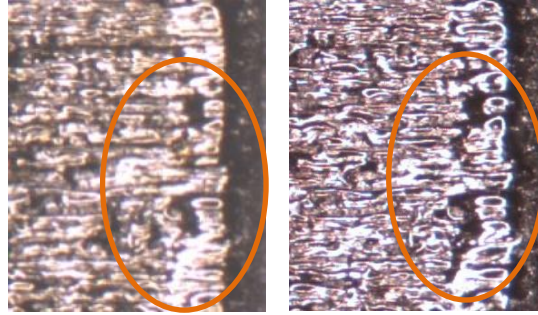


Figure 7- An example of image in which local image saturation has covered local surface features compared to microscope. Left: camera, right: microscope.

Automated Detection of Pores from Camera Images

After the imaging setup enables to capture in-situ images from each layer that visualize detailed surface features and pores, automatic detection of defects can be performed. To detect pores individually in an automatic manner, appropriate image processing algorithms should be developed. The developed algorithms would have some level of performance in terms of false alarms or false negatives that could be satisfactory or insufficient for a given application or a specific build. The development and the performance of algorithms would strongly depend on the characteristics and clarity of images, the visibility, contrast, and discriminability of pores compared to the background and non-defective regions, the level of noise, etc.

By observing camera and microscopic images of different layers, it is seen that the part surfaces have some discolored regions that appear brown on the surface (see Figure 8). These brown regions are believed to have been formed due to oxidation with the small amounts of Oxygen in the chamber or the gas bubbles in the powder grains [10]. The level of oxygen in the chamber was always maintained lower than 500 ppm and mainly at 250 ppm. This oxidation level could significantly be reduced if the build was performed at lower oxygen concentrations such as 100 ppm which is completely feasible. These brown regions, also called darkly etching regions, in images, look like pores in the layers and, unless closely observed, they can sometimes easily be mistaken with pores by visual observation of the images with human eye. Therefore, in processing of the images, they also interfere with segmentation of pores and appear as false alarms.

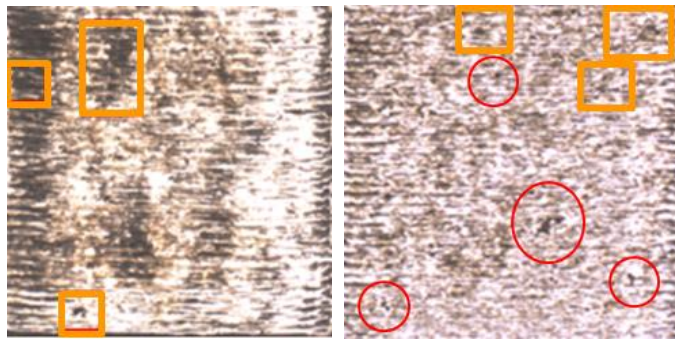


Figure 8- Two example camera images that show a smooth pore-less layer (left) and a porous layer (right). Squares mark examples of darkly-etching regions that are of the same color as pores and sometimes have

same characteristic of pores after segmentation, and circles mark examples of true pores. Verification was made by microscopic examination.

For defect detection, image segmentation algorithms are developed with the objective of detection of pores from images. However, due to the large variety of layer characteristics, and surface appearances, and different looks of pores, and darkly etching regions, development of an algorithm to detect individual pores without segmenting surface discolorations and darkly etching spots is very challenging and complicated. Therefore, the image segmentation algorithms that are developed to detect pores consequently detect darkly-etched regions as well. After segmentation of pores and darkly-etched regions, the characteristics of the segmented objects can be used to remove many of these false detections. Additionally, it will be seen that smoother surfaces (built with higher energy) tend to have more and larger darkly-etched regions compared to rougher and porous surfaces (associated with low energy). This observation would suggest that identification of layers that likely have pores (associated with low energy or Zone III as introduced by Starr *et al.* [11, 12]) from layers with smoother surfaces that have very low chances of having pores (optimal or high energy, Zones I and II [11]) would then help to more confidently decide if the segmented objects in the image are pores or darkly etching regions. This identification has been performed and will be briefly presented in the next section.

In the following, appropriate image processing algorithms will be developed to detect pores using intensity-based algorithms. Figure 9 shows an example image of a porous layer. As it is seen, there are some darkly-etching spots that have the same color as pores and even sometimes it is difficult for human eye to distinguish between the two. Pores and these dark spots can very clearly be distinguished by directly looking through microscope with both eyes that can detect depth. Microscopic images also in general show relatively good discrimination between pores and these dark spots. However, due to the reasons mentioned in previous section, camera images do not show the level of clarity of microscopic images.

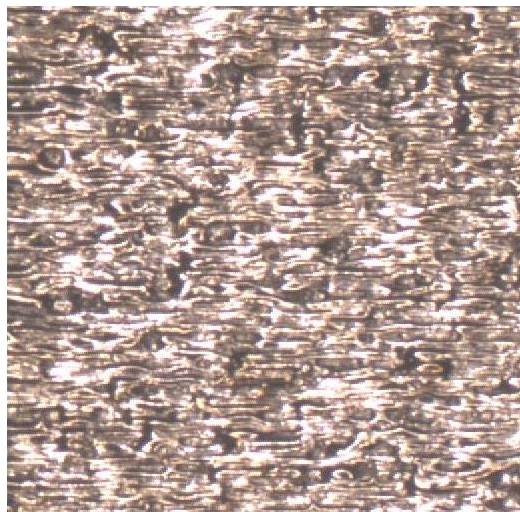


Figure 9- Example image of a porous layer

To start designing segmentation algorithms, we would start with thresholding and would study how pores would appear after implementing different threshold values. Figure 10 show results of thresholding with four different thresholds. A high threshold segments most and larger portions of pores, but it also segments large regions of darkly-etched spots. A low threshold segments fewer darkly-etched spots; however, it doesn't segment all areas of a pore and does not detect some of the small pores at all. It was examined and decided that a low threshold can then be used to detect locations of pores, and a high threshold gives a better estimate of pores shape and size. In other words, the image with a low threshold not too low to segment noisy spots can locate or mark defects and the image with a higher threshold shows the full shape of defects at the markers. This context can be implemented using an image processing algorithm called reconstruction [13]. Therefore, the image with a low threshold (Figure 10 (b)) was used as a marker to signify locations of pores. An image with high threshold, Figure 10 (d), was also used as a mask in the (morphological) reconstruction operation.

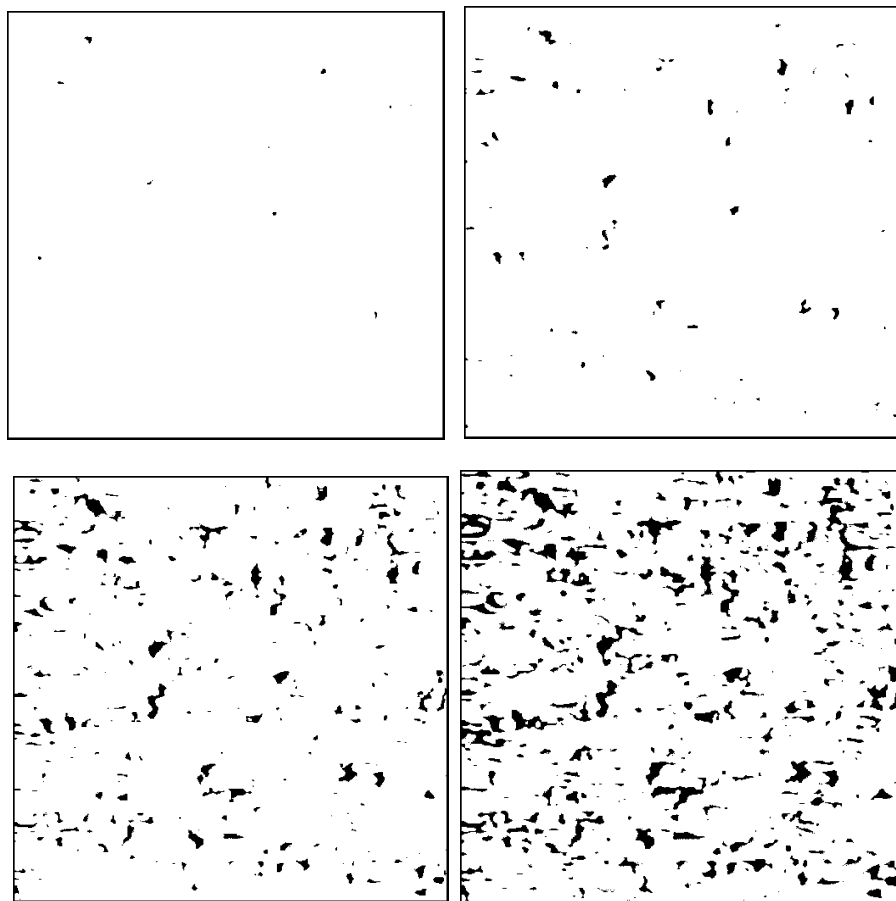


Figure 10- Result of thresholding of wiener-filtered gray-scale image of Figure 9 with different thresholds. The thresholds are: (a) 0.32, (b) 0.35, (c) 0.4, (d) 0.43.

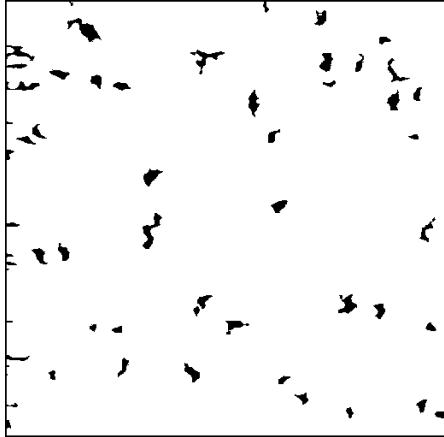


Figure 11- Application of reconstruction to segment pores from the camera image. Figure 10 (b) was used as marker and Figure 10 (d) as mask.

Figure 11 shows the result of reconstruction. The result shows that the majority of pores in the layer are successfully segmented with very few false segmentations. Figure 12 shows the result of implementation of the same algorithm to another examples image. By close visual examination of segmentation results for various images it can be seen that almost all pores larger than 80 microns are segmented in addition to many of the smaller pores. Although applying the same algorithm to other images and layers leads to segmentation of the majority of pores, in some cases, especially towards the higher energy end, several darkly-etching regions are also segmented. It was investigated that it is possible to remove many of these false segmentation by imposing rules on the geometric characteristics of the segmented objects. Identification and removal of these false segmentations and evaluation of the pore segmentation algorithms is among the future work.

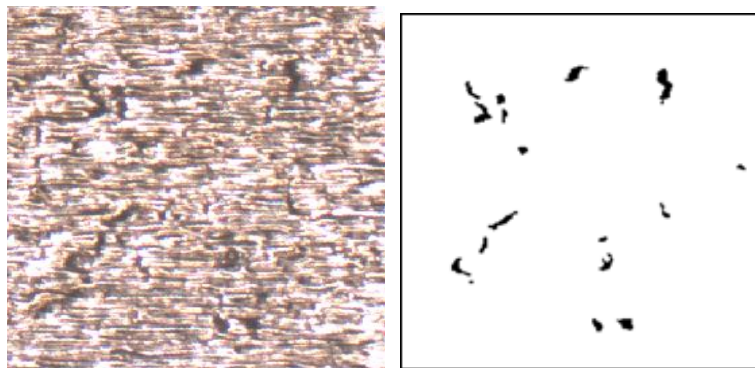


Figure 12- Example of application of the segmentation algorithm to another image of a porous region.

Identification of Porous Regions using Intelligent Pattern-Matching Algorithms

While detection of individual pores using pore segmentation algorithm provides information about layer porosity, it is possible to extract features from the layer that are correlated with porosity and use them in an intelligent identification algorithm to provide a qualitative or even quantitative assessment of porosity. For example, porous layers can be identified versus non-porous layers using such identification. Additionally, the result of identification of porous regions can serve with detection of individual pores, by suggesting which images represent a porous layer to be detected for pores. To perform identification of porous regions, it is possible to use a discriminator associated with non-porous regions and identify them from porous regions. This identification would also serve as a quantitative measure of porosity in the layers and the part as a whole. This would be possible using application of classification algorithms to identify the texture associated with porous regions from non-porous regions. Classification of porous versus non-porous regions was successfully performed and is briefly described in this section.

Figure 13 shows an example image of a smooth, non-porous layer versus a porous layer. It is seen that the smooth surface is associated with smooth variation of intensity and a porous surface is associated with sharp and abrupt variation. Therefore, a feature associated with the spatial variation of intensity would be able to discriminate these surfaces. By study of the behavior of the images in the spatial and frequency domain after implementation of fast Fourier transform, five dominant features were identified that were able to discriminate porous surfaces versus smooth non-porous surfaces.

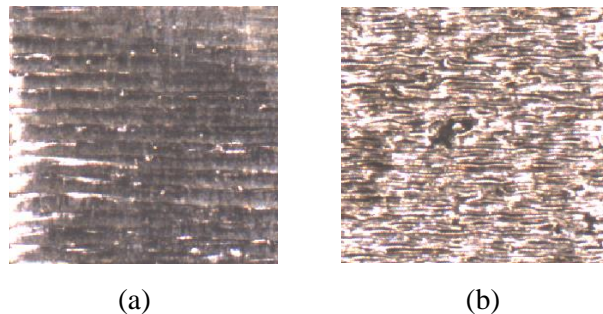


Figure 13- Example images of (a) a smooth surface, and (b) a porous surface.

After choosing discriminating features, a classifier should be chosen and trained. There are a variety of choices of classifiers such as neural network, support vector machine, k-mean clustering, and statistical classifiers such as Bayesian. For this work, a Bayesian network was developed and trained to classify porous versus non-porous surfaces based on over 100 train samples. The performance of the algorithm was then evaluated by implementing the classifier to 100 test sample. The Bayesian classifier was able to identify porous versus non-porous layers with over 90% accuracy.

Conclusions

This paper describes the system and the work on development of a new imaging setup with the collaboration of the Edison Welding Institute (EWI). Unlike the previous and existing work on development of imaging setup for powder-bed AM, this system resolves, to a significant extent, the challenges associated with the illumination and captures images that visualize detailed surface

features such as individual pores as they appear in microscopic images. A movable illumination source is conveniently utilized to illuminate the part surface closely and without blocking the laser power. Appropriate image processing algorithms were developed to detect pores from the part surface automatically and as precisely as possible. In addition to detection of individual pores, an intelligent classification algorithm, based on Bayesian inference, was developed to identify porous versus non-porous layers. The Bayesian network assigns a probability value that shows the likelihood that the inspected layer is porous. The output value can also be used as a measure of the level of porosity of the layer. The developed identification framework can be used similarly to identify and characterize other part attributes such as quality of fusion, layer roughness, and the level of build energy for the layer.

Acknowledgements

The authors would like to thank the Edison Welding Institute for funding this research and providing the equipment and support for conducting this work.

References

1. Craeghs, T., et al. *Online quality control of selective laser melting*. in *20th Solid Freeform Fabrication (SFF) symposium*. 2011. Austin (Texas).
2. Kleszczynski, S., z.J. Joschka, and J.T. Sehart. *Error detection in laser beam melting systems by high resolution imaging*. in *Proceedings of the Twenty Third Annual International Solid Freeform Fabrication Symposium*. 2012.
3. Jacobsm, J.z., et al. *High resolution imaging for inspection of laser beam melting systems*. in *2013 IEEE International Instrumentation and Measurement Technology Conference (I2MTC)*. 2013.
4. zur Jacobsmühlen, J., et al. *Elevated region area measurement for quantitative analysis of laser beam melting process stability*. in *26th International Solid Freeform Fabrication Symposium; Austin, TX*. 2015.
5. Aminzadeh, M. and T. Kurfess, *In-situ monitoring of dimensional accuracy in additive manufacturing by layerwise detection of geometric errors*. 2015.
6. Aminzadeh, M. and T. Kurfess. *Layerwise Automated Visual Inspection in Laser Powder-Bed Additive Manufacturing*. in *ASME 2015 International Manufacturing Science and Engineering Conference*. 2015. American Society of Mechanical Engineers.
7. Aminzadeh, M. and T. Kurfess. *Vision-based inspection system for dimensional accuracy in powder-bed additive manufacturing*. in *ASME 2016 International Manufacturing Science and Engineering Conference*. American Society of Mechanical Engineers. 2016.
8. Foster, B., et al. *Optical, layerwise monitoring of powder bed fusion*. in *26th International Solid Freeform Fabrication Symposium; Austin, TX*. 2015.
9. zur Jacobsmuhlen, J., et al. *Robustness analysis of imaging system for inspection of laser beam melting systems*. in *Emerging Technology and Factory Automation (ETFA), 2014 IEEE*. 2014. IEEE.
10. Prabhu, A.W., *Improving Fatigue Life of LENS Deposited Ti-6Al-4V through Microstructure and Process Control*. 2014, The Ohio State University.
11. Gong, H., et al., *Analysis of defect generation in Ti-6Al-4V parts made using powder bed fusion additive manufacturing processes*. *Additive Manufacturing*, 2014. **1**: p. 87-98.

12. Gong, H., et al. *Defect Morphology in Ti–6Al–4V Parts Fabricated by Selective Laser Melting and Electron Beam Melting*. in *24rd Annual International Solid Freeform Fabrication Symposium—An Additive Manufacturing Conference, Austin, TX, Aug. 2013*.
13. Shapiro, L.G. and G.C. Stockman, *Computer Vision*. 2001, London Prentice Hall.